New Details of the Human Corneal Limbus Revealed With Second Harmonic Generation Imaging

Choul Yong Park,[1,2] Jimmy K. Lee,[2] Cheng Zhang,[2] and Roy S. Chuck[2]

[1]Department of Ophthalmology, Dongguk University, Ilsan Hospital, Goyang, Kyunggido, South Korea
[2]Department of Ophthalmology and Visual Sciences, Montefiore Medical Center, Albert Einstein College of Medicine, Bronx, New York, United States

Correspondence: Roy S. Chuck, Department of Ophthalmology and Visual Sciences, Montefiore Medical Center, Albert Einstein College of Medicine, Bronx, NY 10467, USA; rchuck@montefiore.org.

CYP and JKL contributed equally to the work presented here and should therefore be regarded as equivalent authors.

Submitted: March 2, 2015
Accepted: August 12, 2015

Citation: Park CY, Lee JK, Zhang C, Chuck RS. New details of the human corneal limbus revealed with second harmonic generation imaging. *Invest Ophthalmol Vis Sci*. 2015;56:6058–6066. DOI:10.1167/iovs.15-16783

Purpose. To report novel findings of the human corneal limbus by using second harmonic generation (SHG) imaging.

Methods. Corneal limbus was imaged by using an inverted two-photon excitation fluorescence microscope. Laser (Ti:Sapphire) was tuned at 850 nm for two-photon excitation. Backscatter signals of SHG and autofluorescence (AF) were collected through a 425/30-nm emission filter and a 525/45-emission filter, respectively. Multiple, consecutive, and overlapping image stacks (z-stack) were acquired for the corneal limbal area.

Results. Two novel collagen structures were revealed by SHG imaging at the limbus: an anterior limbal cribriform layer and presumed anchoring fibers. Anterior limbal cribriform layer is an intertwined reticular collagen architecture just beneath the limbal epithelial niche and is located between the peripheral cornea and Tenon's/scleral tissue. Autofluorescence imaging revealed high vascularity in this structure. Central to the anterior limbal cribriform layer, radial strands of collagen were found to connect the peripheral cornea to the limbus. These presumed anchoring fibers have both collagen and elastin and were found more extensively in the superficial layers than deep layer and were absent in very deep limbus near Schlemm's canal.

Conclusions. By using SHG imaging, new details of the collagen architecture of human corneal limbal area were elucidated. High resolution images with volumetric analysis revealed two novel collagen structures.

Keywords: cornea, collagen, limbus, second harmonic generation

Cross-sectional imaging of the cornea and anterior segment has evolved rapidly in recent years. High resolution imaging is now available with optical coherence tomography and high frequency ultrasound tomography.[1–3] Additionally, in vivo confocal microscopy is capable of providing high resolution axial cross-sectional images of corneal cells, nerves, and pathogens.[3–6] However, finer structures, such as interconnecting collagen fibers, are not as well characterized with current modalities.[7]

Second harmonic generation (SHG) imaging was introduced in the 1970s.[8] Second harmonic generation allows study of collagen at submicron scale with minimal invasiveness.[9] Second harmonic generation occurs when the electric field of excitation light is strong enough to deform a molecule.[10] If the molecule is asymmetric, the resulting anisotropy creates an oscillating field at twice the frequency and generates a single photon with half the wavelength and twice the energy of incident photons, a phenomenon termed second harmonic generation.[10] Second harmonic generation is unique to noncentrosymmetric molecules such as collagen. Four types of collagen (I, II, III, and V) form fibrils.[7] Type I collagen, in particular, is highly crystalline and effectively generates the second harmonic.[11,12] It is the major component of cornea (68% of the dry weight) and sclera (70% of the dry weight).[7]

Second harmonic generation imaging performs optical sectioning and three-dimensional (3D) analysis at the submicron level and has several advantages compared to other high resolution images, such as confocal and electron microscopy.[13–17] Fixation and staining are not necessary for SHG imaging, and it is possible to image in vivo. As it is based on nonlinear scatter rather than the absorption of photon energy, SHG does not dissipate energy and spares the sample from excitation, bleaching, or damage.[17,18] Furthermore, near-infrared excitation wavelengths used in SHG imaging allows deeper imaging depth, over 1000 μm.[16–18]

There have been recent reports on SHG imaging of animal and human corneal collagen.[15,19–22] It can detect corneal or scleral collagen by collecting forward[14,19] or backward[14,20,22] SHG signals. In addition to detailing normal anatomy, SHG is effective in distinguishing the differences in pathological conditions, such as bullous keratopathy or keratoconus.[13,14] Changes induced by cross-linking (riboflavin plus UV-A) have been detected with SHG in porcine, rabbit, and bovine corneas.[15,20] Its resolution is lower than that of electron microscopy; however, SHG is capable of volumetric analyses of collagen fiber orientation and 3D interpretation.[22,23] The combination of SHG and autofluorescence (AF) in two-photon excitation fluorescence microscopy enables the detection of collagen and elastin structures simultaneously.[24,25]

The limbus is the transition zone between transparent cornea and opaque sclera in conjunction with a change in the radius of curvature from steeper cornea to flatter sclera. The

Table 1. Clinical Characteristics of Donor Corneal Tissue Used in This Study

Sample No.	Age	Race	Sex	Laterality	Harvest to Imaging Time, d	Clinical History
1	55	White	Female	OD	5	Hypertension, seizure
2	55	White	Female	OS	5	Hypertension, seizure
3	66	White	Male	OD	4	Hypertension, guttata
4	60	White	Female	OD	5	Asthma, glaucoma
5	60	White	Female	OS	5	Asthma, glaucoma
6	14	Black	Male	OD	11	Hypoxic encephalopathy, chronic ICU care
7	14	Black	Male	OS	11	Hypoxic encephalopathy, chronic ICU care

ICU, intensive care unit; OD, oculus dexter; OS, oculus sinster.

current understanding of collagen arrangement in the corneal limbus comes from x-ray diffraction study.[26,27] Several studies have found that a circumcorneal annulus of collagen fibrils is anchored in the limbal region. Although x-ray diffraction technology detects collagen orientation, its use is limited as it does not actually image architectural details.[28]

In this study, serial high-resolution axial images of collagen in the human limbal region were obtained by SHG imaging. By analyzing collagen arrangement in image planes separated by micrometers, new details in the anatomy of the corneal limbus were discovered.

Materials and Methods

This study was approved by the institutional review board of the Albert Einstein College of Medicine, Yeshiva University and adhered to the tenets of the Declaration of Helsinki. Seven eye bank corneas, which were not suitable for human transplantation, were obtained from the Central Florida Lions Eye and Tissue Bank (Tampa, FL, USA).

Sample Preparation

Eye bank corneas were stored in Optisol GS (Bausch & Lomb, Rochester, NY, USA) solution until imaged. At the two-photon microscope, corneas were transferred to a glass-bottom dish (35 mm, MatTek, Ashland, MA, USA) and several drops of balanced salt solution (BSS; Alcon, Fort Worth, TX, USA) were applied to the samples to prevent desiccation. To image the epithelial side, the sample corneal button was placed upside down, with the epithelium against the glass bottom. To image the endothelial side, trabecular meshwork, and deep limbal lamellae, corneal buttons were positioned right-side up, with the endothelium facing the glass bottom.

Two-Photon Excitation Fluorescence Microscopic Imaging Process

Second harmonic generation imaging was performed using an inverted two-photon excitation fluorescence microscope (FluoView FV-1000, Olympus, Central Valley, PA, USA; Supplementary Fig. S1). The cornea was placed upside down, the epithelium against the glass-bottom plate (35 mm, MatTek). A rubber ring was used to tilt and slant the cornea into position to image the areas of interest.

Laser (Ti:Sapphire) was tuned at 850 nm and directed through a red dichroic mirror (RDM 690 nm). A 25X (numerical aperture [N.A.] = 1.05) water immersion objective was used to focus the excitation beam and to collect backscatter signals. The backward signal of SHG was collected through a 425/30-nm emission filter after being reflected by a dichroic mirror (dm458), and the backward signal of AF was collected through a 525/45-nm emission filter after passing through a second dichroic mirror (dm560). Autofluorescence signal obtained with the 525/45-nm filter contains contributions from flavin adenine dinucleotide (FAD), nicotinamide adenine dinucleotide (NADH), and elastin.

A square image (513 μm × 513 μm) was acquired with 1024 × 1024 pixels of resolution in approximately 15 seconds. Multiple, consecutive, and overlapping image stacks (z-stack) were acquired using the same objective lens. When images were z-stacked, samples were scanned in 1- to 10-μm steps in the *z*-axis to generate 3D data sets. For reference, 0-μm position in depth corresponds to the first Z-position where SHG signal is detected. ImageJ software (http://imagej.nih.gov/ij/; provided in the public domain by the National Institutes of Health, Bethesda, MD, USA) was used to analyze acquired images.

Histology and Phalloidin Staining

A piece of corneal tissue was fixed (2% paraformaldehyde + 2.5% glutaraldehyde in 0.1 M cacodylate buffer), dehydrated with ethanol, and embedded with Epon 812. Semithin sections (1 μm) were stained with 1% Toluidine Blue. Another piece of corneal tissue was fixed with methanol free 4% paraformaldehyde. Cells were permeabilized with 0.1% Triton X-100. Fluorescent phallotoxin (Alexa Fluor 488 Phalloidin, catalog number A12379, Life Technologies, Grand Island, NY, USA) was diluted with phosphate-buffered saline containing 1% bovine serum albumin (phallotoxin final concentration of 5 unit/mL) and applied for 20 minutes. Hoechst 33342 (catalog number 62249, Life Technologies) was used to counter stain nuclei. The fluorescent signal was detected with a FluoView FV-1000 microscope.

Results

Demographics and clinical information of donors used in this study are shown in Table 1.

Comparison Between AF and SHG

Autofluorescence, SHG, and merged images of the limbus are shown in Figure 1. Compared to SHG, AF images showed greater fluorescence of cellular architecture, especially cytoplasm and vessels as opposed to collagen structures. In the merged image (Fig. 1C), it is clear that the high-signal structures in AF and SHG are different. This finding is consistent with previous reports.[29,30] In SHG images, collagen structures were noticeably visible with intense signals (Figs. 1A, 1D), whereas cellular structures and vessels were not as evident (Figs. 1B, 1E). Furthermore, the resolution in SHG was high enough to detail the arrangement pattern and direction of the bundled collagen fibers.

Investigative Ophthalmology & Visual Science

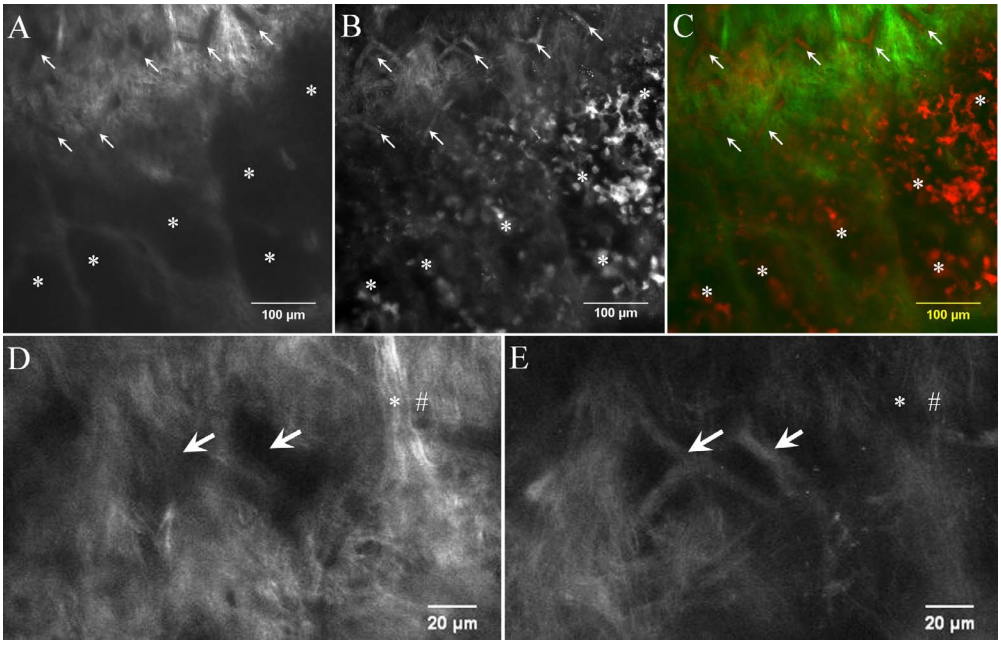

Figure 1. Comparison of AF images and SHG images at the limbus. Autofluorescence image and SHG image were captured at the same focal plane for comparison. (**A**) Collagen structures of limbus yield high SHG signal intensity. The direction of each collagen fiber bundle is visible in the SHG image. The signal void area in SHG (*arrows* and *asterisk*) indicates no collagen structure in this area. (**B**) AF image of the identical limbal region reveals high signal from vessels (*arrows*) and cells (*asterisks*). (**C**) Merged image of panels **A** (pseudocolor *green*) and **B** (pseudocolor *red*) clearly shows that vessels and cells occupy signal-void areas of SHG. (**D**, **E**) Magnified images show collagen intensity is high in SHG (**D**) but is low in AF images (*) (**E**). High intensity fiber in AF is low in SHG (#). Images were taken from sample no. 1.

Palisade of Vogt (PV) Structure

The SHG image of the PV is demonstrated in Figure 2. Their finger-like dark processes extend from the corneal epithelium, alternating with conjunctival subepithelial connective tissue processes, comprised of dense and wavy fibrovascular tissue (Figs. 2A, 2B). Each conjunctival stromal process is highly vascularized with a core vessel trunk and a vascular loop at the leading edge. Tenon's collagen fibers in the PV region appear straight and dense compared to Tenon's collagen in the periphery, over the pars plana region (Figs. 2C, 2D).

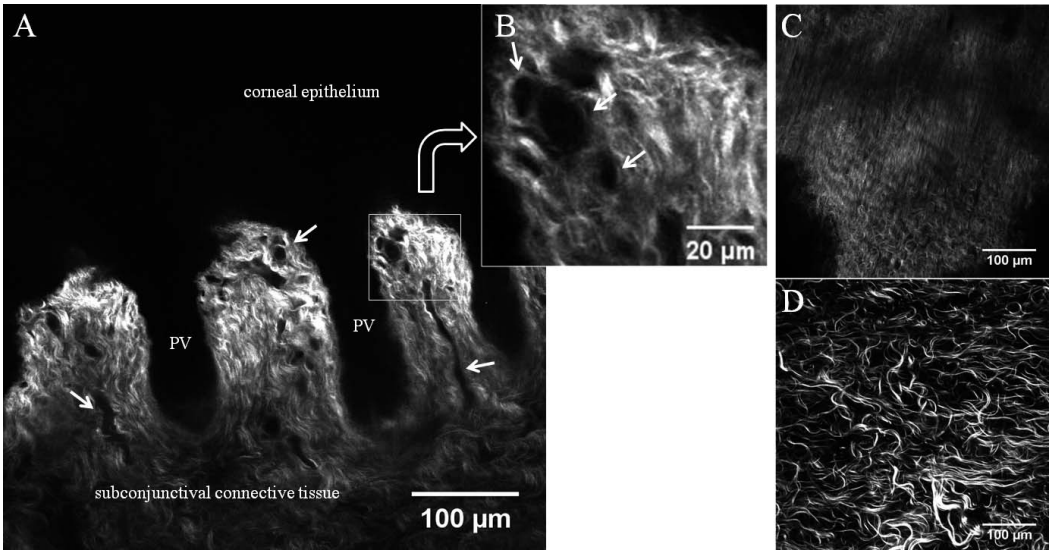

Figure 2. Second harmonic generation images of the PV acquired 10 μm below the surface epithelium. (**A**) Dark, signal-void projections depict corneal epithelial processes (PV), as the PV contains multiple layers of epithelial and limbal stem cells. Interspersed subconjunctival connective tissue processes contain dense, wavy collagen fibers with vascular loops at the tip. (**B**) A square area is magnified and arrows indicate a vascular trunk and loop. (**C**) Collagen arrangement of Tenon tissue near the PV is linear and compact. (**D**) Collagen arrangement of Tenon tissue over the pars plana region is comparatively disorganized and loose. Images were taken from sample no. 2.

Investigative Ophthalmology & Visual Science

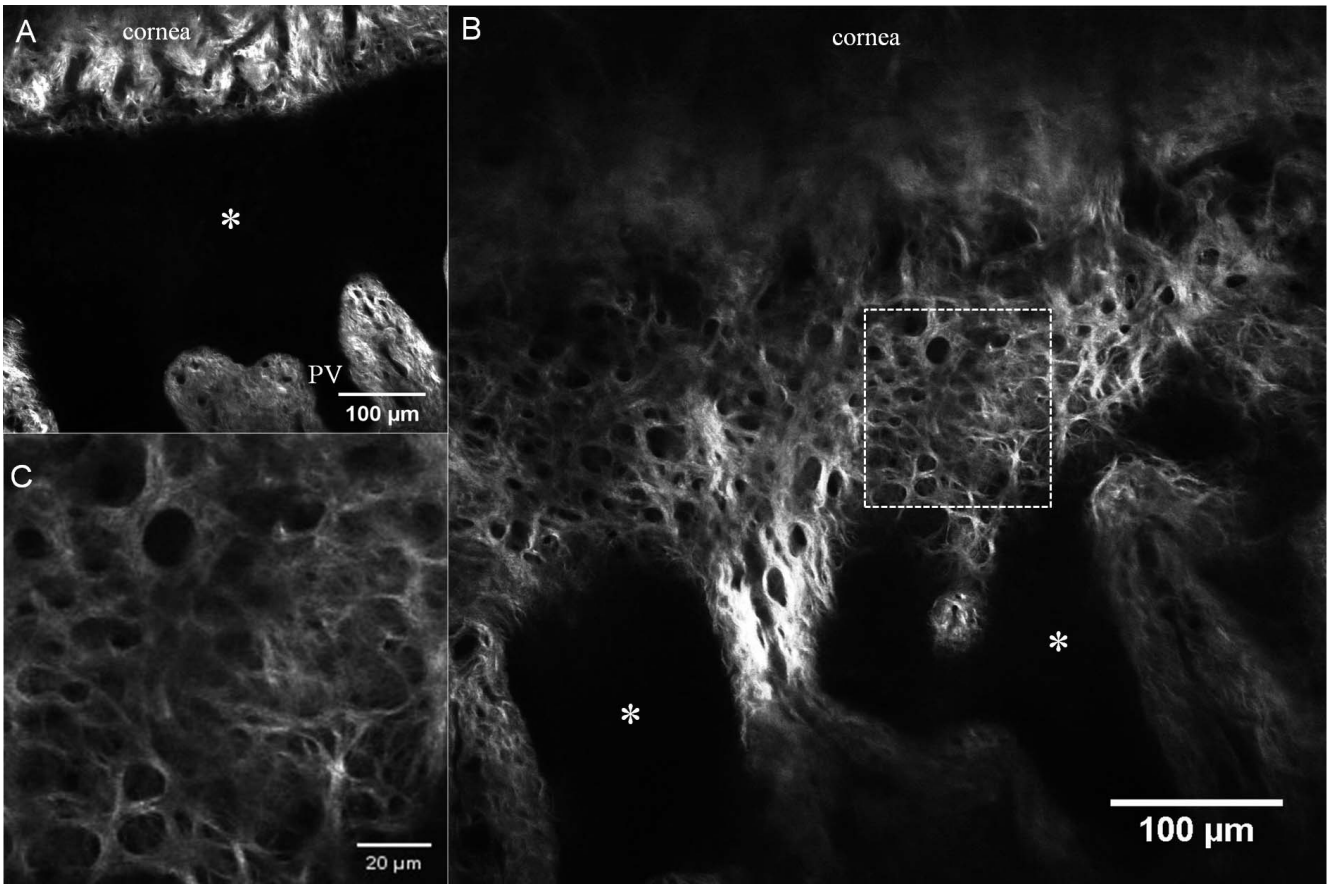

Figure 3. Second harmonic generation images taken 20 μm below the surface epithelium. (**A**) PV (*) is visible between the peripheral cornea and conjunctival processes. (**B**) SHG images taken 40 μm below the surface epithelium. Newly discovered "anterior limbal cribriform layer" bridges the peripheral cornea to conjunctival processes. Its reticular network of collagen (*square area*) is magnified in panel **C**. Images were taken from sample no. 3.

Limbal Epithelial Niche and Collagen Arrangement

The limbal epithelial niche consists of layers of epithelium and underlying stem cells. Located between the cornea and conjunctiva, and this plane was thought to be devoid of SHG signals. However, in this study, an interesting collagen network was discovered just beneath the bottom of this niche, an "anterior limbal cribriform layer." Collagen fibers in this anterior limbal cribriform layer were intertwined in a reticular pattern (Figs. 3, 4) and exhibited similar patterns in each donor tissue (Fig. 5). The location was consistent: between the peripheral cornea and Tenon's tissue superficially, and between the relatively deeper cornea and sclera (Fig. 6; Supplementary Figs. S2, S3). The thickness of the anterior limbal cribriform layer ranged from 20 to 50 μm by tracing z-stack layers. The unique collagen structure of the anterior limbal cribriform layer was not obvious with Toluidine Blue stain histologic sectioning (Supplementary Fig. S4). However, immunostaining of cells with phalloidin in conjunction with SHG elucidated the spatial orientation of the limbal epithelial cells and the anterior limbal cribriform layer (Supplementary Fig. S5).

A Novel Collagen Pattern

Where the anterior limbal cribriform layer connects to the peripheral cornea, the limbal vasculature terminates by forming a large loop. Beyond this vascular loop, a novel collagen pattern was discovered (Fig. 7; Supplementary Fig. S3). These fibers frequently converged within the peripheral cornea and were noted more frequently in superficial layers (Figs. 7B–E; Table 2). They were evident in SHG images down to 170 μm from the surface, but it is challenging to differentiate beyond this depth secondary to decreased signals. Near the origin of these fibers at limbus, abundant autofluorescent positive fibers were also found (Fig. 7G). There was no difference in this fiber density when comparing all four quadrants of the limbus. These novel collagen fiber patterns were not observed in the deeper corneo-scleral junction (Fig. 8) near the trabecular meshwork and Schlemm's canal. In this deeper section of the limbus, an irregular corneal collagen pattern gradually blended to a disorganized arrangement, characteristic of the sclera.

Discussion

In this study, we employed SHG imaging and discovered new details of the human corneal limbus: specifically, a novel cribriform layer of collagen at the superficial limbus and collagen fibers that anchor the peripheral cornea to the limbus.

Axial-sectional confocal microscopy using reflective difference is commonly utilized in clinical ophthalmology and research. The most widely used confocal microscopes are the Confoscan series (Nidek Co. Ltd., Gamagori, Japan) and the Heidelberg Retinal Tomograph/Rostock Cornea Module (Hei-

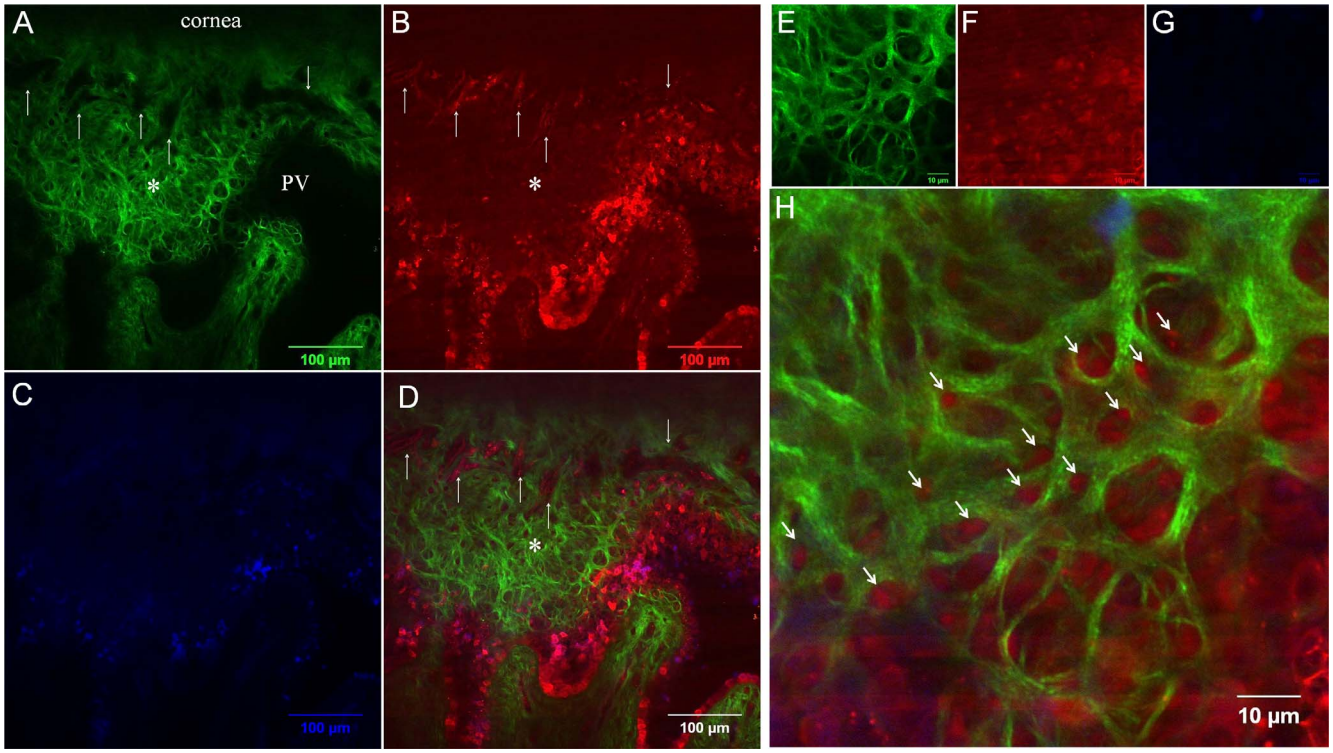

Figure 4. Comparison of SHG (**A**, **E**) and AF (**B**, **F**) images at anterior limbal cribriform layer. (**C**, **G**) 4',6-diamidino-2-phenylindole (DAPI) and (**D**, **H**) merged images. (**A**–**D**) Images taken at 30 μm depth below the epithelium. The anterior cribriform layer is prominent in the SHG image (**A**, *asterisk*). Dark signal-void areas (*arrows*) in the SHG image (**A**) were occupied by AF-positive structure (**B**). DAPI was used to counterstain nucleus (**C**). Merged image (**D**) clearly demonstrates the orientation of collagen and vessels. (**E**–**H**) Magnified images of anterior limbal cribriform layer. *Arrows* indicate the AF positive structure occupying each honeycomb space of anterior limbal cribriform layer. Colors are pseudocolors. Images were taken from sample no. 4.

delberg Engineering GmbH, Heidelberg, Germany).[31] High-resolution axial images of cells and nerves provide important information for accurate diagnosis of corneal diseases, such as limbal stem cell deficiency and various keratitis.[32–35] However, these clinical confocal microscopies use reflection as contrast. Although they adequately outline boundaries such as cellular membranes, it is difficult to image detailed collagen-based structures of cornea.[29] Compared to confocal microscopy, SHG

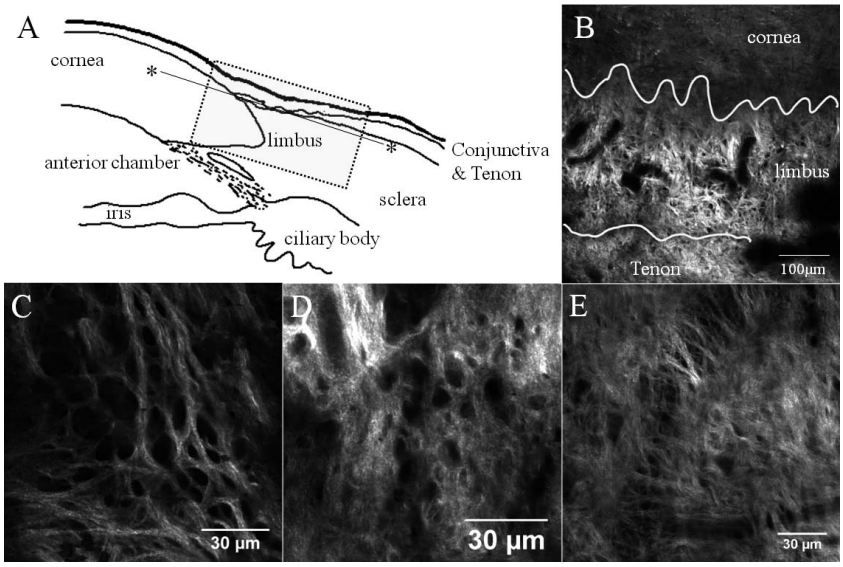

Figure 5. Patterns of anterior limbal cribriform layer at the limbal area. (**A**) Orientation diagram. Dotted box outlines the limbus and the solid line marks the imaging plane (*). (**B**) SHG image obtained at 30 μm depth below the epithelium. Lines divide cornea, limbus, and conjunctiva/Tenon tissue. (**C**–**E**) Anterior limbal cribriform layer from three different donor corneas. Images were taken at 30 μm (**B**), 20 μm (**C**), 24 μm (**D**), and 26 μm (**E**) depth. Images were taken from sample no. 1 (**B**, **C**), no. 5 (**D**), and no. 6 (**E**).

Investigative Ophthalmology & Visual Science

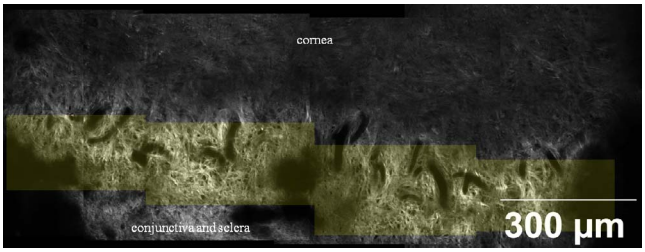

Figure 6. A montage of SHG images taken at 45 µm depth below the epithelium. *Yellow* tint represents anterior limbal cribriform layer. This structure is clearly distinguished from adjacent structures, such as cornea and sclera. Cribriform area spanned 360 degrees around the limbus. Images were taken from sample no. 1.

imaging more clearly defines collagen-containing structures with minimal interference from cells, nerves, and vessels.[13,23,36] It is from these images that we were able to gain a better understanding of the corneal collagen architecture.

One structure that has been elucidated is the PV. Previous studies using confocal microscopy focused on cellular components of the PV: bright and dark cells, corpuscular particles, dendritic cell morphology, and hyperreflective cells.[33,37] However, in this study, SHG has allowed a detailed view of the collagen layout of this region. Conjunctival processes were noted to form islands and route small blood vessels to the PV region. The hyperreflective parallel extensions with internal acellular regions, described in previous confocal studies, may actually correspond to this conjunctival process seen in SHG.[37]

In this study, we also discovered a novel collagen structure at the superficial limbus: an anterior limbal cribriform layer that, to the best of our knowledge, has not been reported before. Because SHG imaging is relatively new, it is possible that studies using reflective confocal microscopy, electron microscopy, and conventional hematoxylin and eosin staining missed this particular collagen layer. The interference from the cellular AF, difficulty with electron microscopy to identify 3D structures, and conventional light microscopy are all possible barriers to visualizing this anterior limbal cribriform layer. The unique advantages of SHG imaging, deep penetration of the laser with minimal tissue damage and serial axial optical

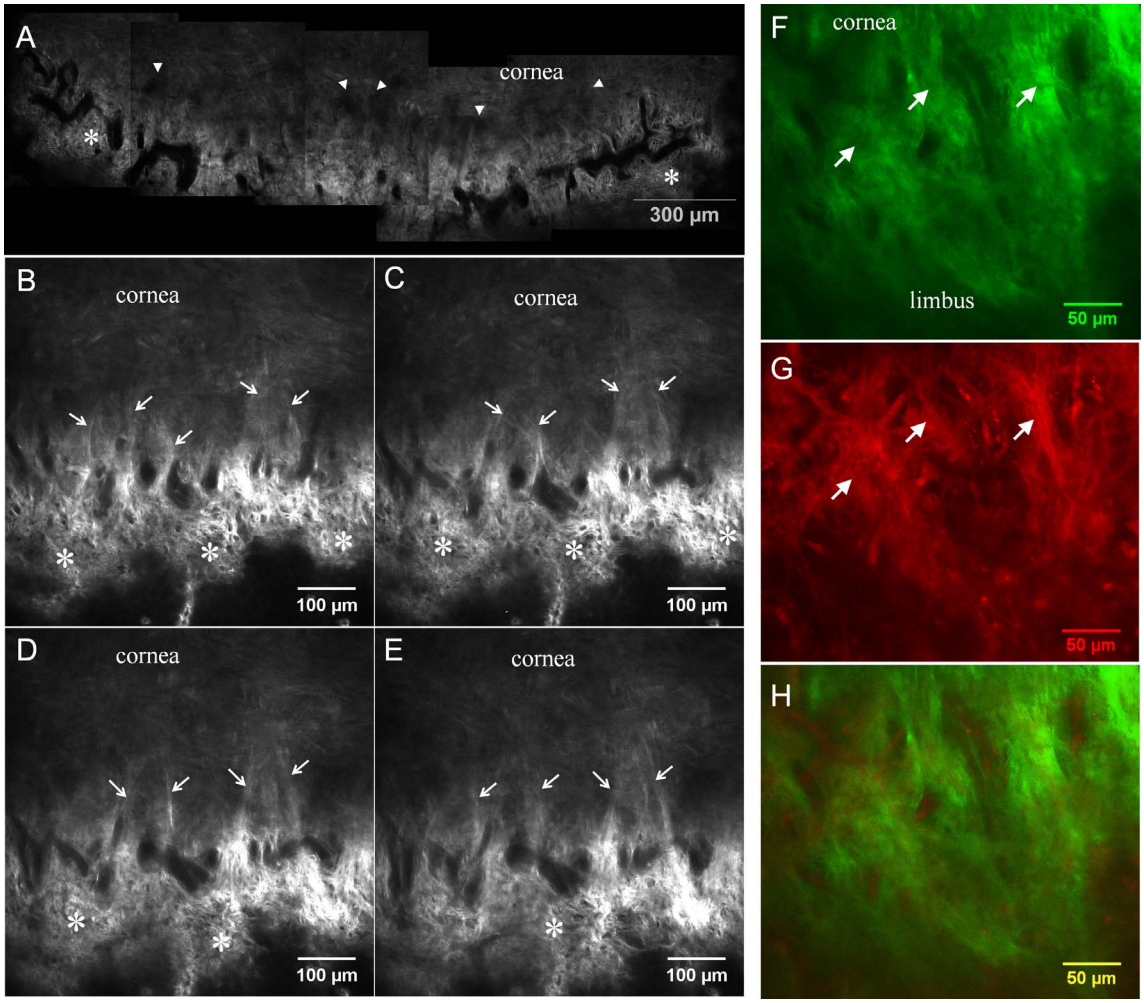

Figure 7. Second harmonic generation images taken at the peri-limbal peripheral cornea. (**A**) A montage image taken 40 µm below the surface epithelium. Prominent vascular structures are visible (dark signal void areas). These vessels surround the entire cornea and form a vascular loop. Part of the anterior limbal cribriform layer (*) is visible adjacent to vascular loop. Dark zone exists between the vascular loop and corneal collagen (*arrowheads*). (**B–E**) On higher magnification, collagen strands (*arrows*) connect the peripheral cornea to the limbus, bridging across this dark zone. Serial Z-section SHG images (5-µm steps) tracing presumed anchoring collagen fibers (*arrows*). (**F–H**) The presence of high AF positive fibers (*arrows* in **F**, **G**) with collagen at the origin of presumed anchoring fibers was demonstrated. (**F**) SHG, (**G**) AF, and (**H**) merged. Images were taken from sample no. 1.

Investigative Ophthalmology & Visual Science

Table 2. Connection Fiber Analysis

Quadrant	Density (Number Per Image)		*P* Value
Superior	Superficial	11.20 ± 077	<0.001
	Deep	6.26 ± 0.78	
Inferior	Superficial	10.91 ± 1.02	<0.001
	Deep	6.46 ± 1.12	
Temporal	Superficial	10.93 ± 1.02	<0.001
	Deep	6.26 ± 1.16	
Nasal	Superficial	10.73 ± 1.03	<0.001
	Deep	6.33 ± 0.62	

The number of connection fibers was manually counted from a square of image (513 μm × 513 μm). Five areas were selected from images taken at 50 μm (superficial) and 120 μm (deep) below zero plane at each quadrant. The pooled analysis of seven donor tissues was demonstrated in this table. *P* values were calculated using independent *t*-test.

sectioning without a fixative, may have permitted discovery of this new structure. Interestingly, the anterior limbal cribriform layer is only approximately 50 μm thick and localized only to the superficial layer of the limbus just beneath the PV. We observed that some of the cribriform spaces are occupied by autofluorescent and phalloidin staining-positive structures. We suspect that this delicate collagen structure may serve as a suspension system, buffering some mechanical stress. In addition, the reticular pattern of the cribriform layer may also be conducive to an abundant vascular supply for the limbal niche area.

With SHG, we also found numerous presumed anchoring collagen fibers in the limbal region. These fibers originate near the vascular loop adjacent to the cribriform layer and run radially into the peripheral cornea, merging with the corneal lamellae. These connection fibers were distributed more densely in the superficial area. The collagen arrangement of human cornea is more complex in the anterior lamellae near Bowman membrane with more fiber interconnections than the posterior lamellae.[23] Previous studies using x-ray diffraction have theorized the existence of anchoring collagen fibers connecting the cornea, limbus, and sclera.[28,38] Although x-ray diffraction quantitatively determines the bulk thickness orientation of collagen fibers, 3D architecture is extrapolated from the preferential orientation data. Various models to elucidate corneal and limbal integration have been proposed by different researchers.[39–41] Recently, Winkler et al.[23] analyzed mosaic SHG images of the serial sagittal sections of human cornea and found a long prominent collagen fiber originating from limbus and extending for several millimeters across the cornea. This fiber ran in a straight line rather than following the corneal curvature. Our findings of presumed anchoring collagen fibers have similar characteristics. The fibers are straight, long, and originate from the limbal region. These fibers are more clearly depicted in our study by using axial z-stack images without tissue fixatives. While analyzing sagittal images may provide better understanding of collagen fiber change along the depth of corneal thickness, the distribution and density of specific collagen structures can be more visible in serial axial images. The images from this study and Winkler et al.[23] confirm the existence of the anchoring fibers, which had been suggested by prior x-ray diffraction studies. It is of note that our "presumed anchoring fiber" is different from the "anchoring fibril" proposed by Kenyon et al.[42] and Gipson et al.[43] Anchoring fibril is a component of an adhesion complex, which attaches to the corneal epithelial basement membrane from the stromal side.

Deeper in the limbus, near Schlemm's canal, typical corneal and scleral collagen fiber arrangements were found. The orientation of peripheral corneal collagen fibers were tangential as shown in Figure 8B. This pattern distinctly differs from disorganized scleral collagen fibers and is consistent with previous x-ray diffraction studies.[28] However, no anchoring fibers were found in the deep corneo-scleral junction.

In summary, we have elucidated the collagen architecture of the human corneal limbus with SHG imaging. The high-resolution images revealed a novel anterior limbal cribriform layer and novel presumed anchoring fibers. The clinical relevance of the two can be interesting topics for further investigation. Additionally, by being minimally invasive, SHG imaging has the potential to be a powerful diagnostic tool for anterior segment diseases.

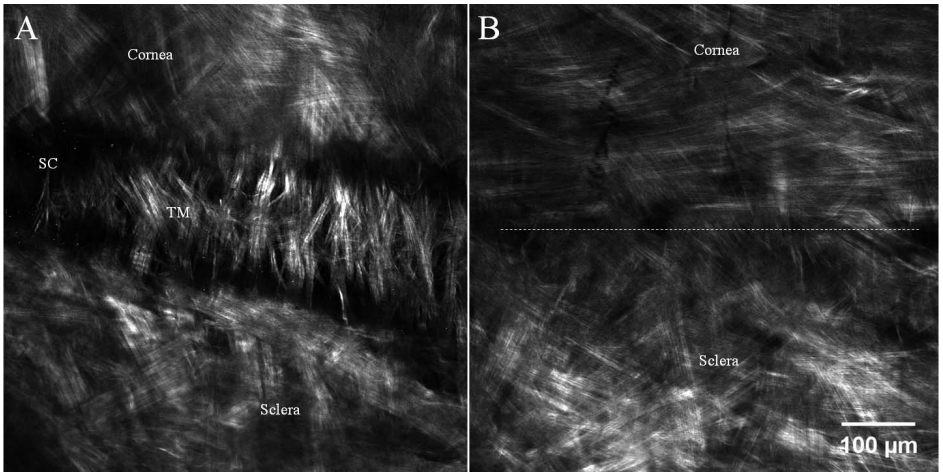

Figure 8. Second harmonic generation imaging from the endothelial side. (**A**) Aqueous outflow system is observed between cornea and sclera. The trabecular structure (TM) consists of the inner wall of Schlemm's canal (SC). (**B**) Cornea-sclera junction taken 100 μm above outer wall of Schlemm's canal. Dotted line roughly divides the corneal collagen and scleral collagen. Note the different collagen arrangement between cornea (more organized) and sclera. Peripheral corneal collagen is arranged in tangential and circumferential pattern. Images were taken from endothelial side and from sample no. 7.

Acknowledgments

The authors thank Central Florida Lions Eye and Tissue Bank (Tampa, FL, USA) for their generous tissue support and Peng Guo, PhD, of Analytical Imaging Facility, Albert Einstein College of Medicine for kind technical assistance related to imaging process.

Supported in part by the Basic Science Research Program (CYP) through the National Research Foundation of Korea (NRF) funded by the Ministry of Education, Science, and Technology (NRF 2010-0002532), Dongguk University Research Fund of 2014 (CYP), a core grant (RSC) from Research to Prevent Blindness (Albert Einstein College of Medicine), and the NCI cancer center support grant (P30CA013330) for Analytical Imaging Facility of the Albert Einstein College of Medicine. The authors alone are responsible for the content and writing of the paper.

Disclosure: **C.Y. Park**, None; **J.K. Lee**, None; **C. Zhang**, None; **R.S. Chuck**, None

References

1. El Sanharawi M, Sandali O, Basli E, et al. Fourier-domain optical coherence tomography imaging in corneal epithelial basement membrane dystrophy: a structural analysis. *Am J Ophthalmol*. 2015;159:755–763.
2. Reinstein DZ, Gobbe M, Archer TJ. Anterior segment biometry: a study and review of resolution and repeatability data. *J Refract Surg*. 2012;28:509–520.
3. Villani E, Baudouin C, Efron N, et al. In vivo confocal microscopy of the ocular surface: from bench to bedside. *Curr Eye Res*. 2014;39:213–231.
4. Kheirkhah A, Dohlman TH, Amparo F, et al. Effects of corneal nerve density on the response to treatment in dry eye disease. *Ophthalmology*. 2015;122:662–668.
5. Bucher F, Hos D, Matthaei M, Steven P, Cursiefen C, Heindl LM. Corneal nerve alterations after Descemet membrane endothelial keratoplasty: an in vivo confocal microscopy study. *Cornea*. 2014;33:1134–1139.
6. Mantopoulos D, Cruzat A, Hamrah P. In vivo imaging of corneal inflammation: new tools for clinical practice and research. *Semin Ophthalmol*. 2010;25:178–185.
7. Meek KM, Fullwood NJ. Corneal and scleral collagens: a microscopist's perspective. *Micron*. 2001;32:261–272.
8. Hellwarth R, Christensen P. Nonlinear optical microscope using second harmonic generation. *Appl Opt*. 1975;14:247–248.
9. Cicchi R, Vogler N, Kapsokalyvas D, Dietzek B, Popp J, Pavone FS. From molecular structure to tissue architecture: collagen organization probed by SHG microscopy. *J Biophotonics*. 2013;6:129–142.
10. Cox G, Kable E. Second-harmonic imaging of collagen. *Methods Mol Biol*. 2006;319:15–35.
11. Roth S, Freund I. Optical second-harmonic scattering in rat-tail tendon. *Biopolymers*. 1981;20:1271–1290.
12. Campagnola PJ, Loew LM. Second-harmonic imaging microscopy for visualizing biomolecular arrays in cells, tissues and organisms. *Nature Biotech*. 2003;21:1356–1360.
13. Morishige N, Shin-Gyou-Uchi R, Azumi H, et al. Quantitative analysis of collagen lamellae in the normal and keratoconic human cornea by second harmonic generation imaging microscopy. *Invest Ophthalmol Vis Sci*. 2014;55:8377–8385.
14. Morishige N, Yamada N, Zhang X, et al. Abnormalities of stromal structure in the bullous keratopathy cornea identified by second harmonic generation imaging microscopy. *Invest Ophthalmol Vis Sci*. 2012;53:4998–5003.
15. Steven P, Hovakimyan M, Guthoff RF, Huttmann G, Stachs O. Imaging corneal crosslinking by autofluorescence 2-photon microscopy, second harmonic generation, and fluorescence lifetime measurements. *J Cataract Refract Surg*. 2010;36:2150–2159.
16. Zipfel WR, Williams RM, Christie R, Nikitin AY, Hyman BT, Webb WW. Live tissue intrinsic emission microscopy using multiphoton-excited native fluorescence and second harmonic generation. *Proc Natl Acad Sci U S A*. 2003;100:7075–7080.
17. Campagnola P. Second harmonic generation imaging microscopy: applications to diseases diagnostics. *Anal Chem*. 2011;83:3224–3231.
18. So PT, Dong CY, Masters BR, Berland KM. Two-photon excitation fluorescence microscopy. *Ann Rev Biomed Engin*. 2000;2:399–429.
19. Teng SW, Tan HY, Peng JL, et al. Multiphoton autofluorescence and second-harmonic generation imaging of the ex vivo porcine eye. *Invest Ophthalmol Vis Sci*. 2006;47:1216–1224.
20. Bueno JM, Gualda EJ, Giakoumaki A, Perez-Merino P, Marcos S, Artal P. Multiphoton microscopy of ex vivo corneas after collagen cross-linking. *Invest Ophthalmol Vis Sci*. 2011;52:5325–5331.
21. Johnson AW, Ammar DA, Kahook MY. Two-photon imaging of the mouse eye. *Invest Ophthalmol Vis Sci*. 2011;52:4098–4105.
22. Bueno JM, Gualda EJ, Artal P. Analysis of corneal stroma organization with wavefront optimized nonlinear microscopy. *Cornea*. 2011;30:692–701.
23. Winkler M, Chai D, Kriling S, et al. Nonlinear optical macroscopic assessment of 3-D corneal collagen organization and axial biomechanics. *Invest Ophthalmol Vis Sci*. 2011;52:8818–8827.
24. Kamma-Lorger CS, Boote C, Hayes S, et al. Collagen and mature elastic fiber organization as a function of depth in the human cornea and limbus. *J Struct Biol*. 2010;169:424–430.
25. Huang AS, Gonzalez JM Jr, Le PV, Heur M, Tan JC. Sources of structural autofluorescence in the human trabecular meshwork. *Invest Ophthalmol Vis Sci*. 2013;54:4813–4820.
26. Newton RH, Meek KM. The integration of the corneal and limbal fibrils in the human eye. *Biophys J*. 1998;75:2508–2512.
27. Newton RH, Meek KM. Circumcorneal annulus of collagen fibrils in the human limbus. *Invest Ophthalmol Vis Sci*. 1998;39:1125–1134.
28. Boote C, Kamma-Lorger CS, Hayes S, et al. Quantification of collagen organization in the peripheral human cornea at micron-scale resolution. *Biophys J*. 2011;101:33–42.
29. Chen WL, Sun Y, Lo W, Tan HY, Dong CY. Combination of multiphoton and reflective confocal imaging of cornea. *Microsc Res Tech*. 2008;71:83–85.
30. Steven P, Bock F, Huttmann G, Cursiefen C. Intravital two-photon microscopy of immune cell dynamics in corneal lymphatic vessels. *PLoS One*. 2011;6:e26253.
31. Niederer RL, McGhee CN. Clinical in vivo confocal microscopy of the human cornea in health and disease. *Prog Retin Eye Res*. 2010;29:30–58.
32. Nubile M, Lanzini M, Miri A, et al. In vivo confocal microscopy in diagnosis of limbal stem cell deficiency. *Am J Ophthalmol*. 2013;155:220–232.
33. Miri A, Al-Aqaba M, Otri AM, et al. In vivo confocal microscopic features of normal limbus. *Br J Ophthalmol*. 2012;96:530–536.
34. Alhatem A, Cavalcanti B, Hamrah P. In vivo confocal microscopy in dry eye disease and related conditions. *Semin Ophthalmol*. 2012;27:138–148.
35. Kumar RL, Cruzat A, Hamrah P. Current state of in vivo confocal microscopy in management of microbial keratitis. *Semin Ophthalmol*. 2010;25:166–170.

36. Morishige N, Sonoda KH. Bullous keratopathy as a progressive disease: evidence from clinical and laboratory imaging studies. *Cornea*. 2013;32(suppl 1):S77–S83.
37. Patel DV, Sherwin T, McGhee CN. Laser scanning in vivo confocal microscopy of the normal human corneoscleral limbus. *Invest Ophthalmol Vis Sci*. 2006;47:2823–2827.
38. Aghamohammadzadeh H, Newton RH, Meek KM. X-ray scattering used to map the preferred collagen orientation in the human cornea and limbus. *Structure*. 2004;12:249–256.
39. Meek KM, Boote C. The organization of collagen in the corneal stroma. *Exp Eye Res*. 2004;78:503–512.
40. Pinsky PM, van der Heide D, Chernyak D. Computational modeling of mechanical anisotropy in the cornea and sclera. *J Cataract Refract Surg*. 2005;31:136–145.
41. Misson GP. Circular polarization biomicroscopy: a method for determining human corneal stromal lamellar organization in vivo. *Ophthalmic Physiol Opt*. 2007;27:256–264.
42. Kenyon KR, Maumenee AE. The histological and ultrastructural pathology of congenital hereditary corneal dystrophy: a case report. *Invest Ophthalmol*. 1968;7:475–500.
43. Gipson IK, Spurr-Michaud SJ, Tisdale AS. Anchoring fibrils form a complex network in human and rabbit cornea. *Invest Ophthalmol Vis Sci*. 1987;28:212–220.

Investigative Ophthalmology & Visual Science